ParamISP: Learned Forward and Inverse ISPs using Camera Parameters
— *Supplementary Material* —

Woohyeok Kim[1*] Geonu Kim[1*] Junyong Lee[2†]
Seungyong Lee[1] Seung-Hwan Baek[1] Sunghyun Cho[1]
[1]POSTECH [2]Samsung AI Center Toronto

(a) Blurred Input (b) CycleISP (c) InvISP (d) RSBlur (e) RealBlur-J (f) ParamISP (Ours)

Figure S1. Qualitative results of deblurring dataset synthesis. Compared to other methods, the deblurring model [3] trained on the dataset synthesized by our ISP models more effectively restores sharp details.

S1. Overview

In this supplementary material, we describe two additional applications: deblurring dataset synthesis and camera-to-camera transfer (Sec. S2). We then provide details and an ablation study on the input features used in LocalNet and GlobalNet (Sec. S3), as well as additional experiments on the global adjustment operation in GlobalNet (Sec. S4) and additional discussions on the training strategy (Sec. S5). We also provide experimental results on the relationship between optical parameters and ParamNet (Sec. S6). Finally, we present additional quantitative and qualitative results (Sec. S7), along with the detailed architecture of ParamISP (Sec. S8).

S2. Additional Applications

ParamISP can be applied to various applications (*e.g.*, deblurring dataset synthesis, RAW deblurring, HDR reconstruction, and camera-to-camera transfer) unlike previous methods. In this section, we describe two additional applications (*i.e.*, deblurring dataset synthesis, camera-to-camera transfer) that were not covered in the main paper. We find that joint fine-tuning on separately trained forward and inverse ISP networks brings additional performance improvements in applications. Therefore, before applying ParamISP to applications excluding camera-to-camera transfer, we conduct additional joint fine-tuning.

In the joint fine-tuning stage, we train our pretrained forward and inverse ISP networks for 450 epochs with an initial learning rate of 1.0×10^{-4}. We jointly fine-tune separately trained forward and inverse ISP networks in an end-to-end manner using loss $\mathcal{L}_{joint}$:

$$\mathcal{L}_{joint} = \|f_{for}(f_{inv}(I_{sRGB})) - I_{sRGB}\|_1 + \|f_{inv}(I_{sRGB}) - I_{RAW}\|_1, \quad \text{(S1)}$$

* Equal contribution.
† Work done prior to joining Samsung.

Method	Synthetic				Real
	CycleISP [14]	InvISP [13]	RSBlur [10]	ParamISP (Ours)	RealBlur-J [9]
PSNR↑	29.98	31.06	31.16	31.31	**31.82**
SSIM↑	0.8806	0.9134	0.9142	0.9148	**0.9203**

Table S1. Quantitative results of deblurring dataset synthesis. Our dataset synthesis outperforms all the other synthesis methods. While ours still achieves lower performance than the RealBlur-J training set, this is partly due to the photometric misalignment present in the RealBlur-J dataset.

where f_{for} and f_{inv} are the forward and inverse ISP networks, respectively, and I_{sRGB} is an sRGB image. Other training conditions are the same as those explained in Sec. 4 of the main paper.

S2.1. Deblurring Dataset Synthesis

It is essential to reflect the camera ISP in order to synthesize a realistic image restoration dataset such as deblurring datasets [10]. ParamISP can enhance the accuracy of synthetic deblurring datasets as it can more accurately model real-world camera ISPs. Tab. S1 shows a comparison among different dataset synthesis approaches. On the table, RSBlur [10] is a baseline model that uses a simple parametric ISP model, while InvISP [13], CycleISP [14], and ParamISP mean variants of the RSBlur pipeline whose ISP model is replaced by the corresponding ISP models. For fair comparisons, we train the other ISP models according to their respective learning approaches. We synthesize deblurring datasets using each of the approaches on the table, train a deblurring model [3] using each dataset, and evaluate their performance on the RealBlur-J test set [9], which is a real-world blur dataset. The last column of the table represents the results obtained by directly training the deblurring model on the RealBlur-J train set, and we consider this as the upper bound.

As Tab. S1 shows, ParamISP achieves the closest PSNR to the upper bound, outperforming all the other synthesis approaches. Interestingly, InvISP [13] and CycleISP [14] achieve worse performance than RSBlur [10] although they are learnable approaches. This is because they primarily focus on cyclic reconstruction (sRGB-to-RAW-to-sRGB) and are less suitable for applications that manipulate RAW images as described in the main paper. Specifically, CycleISP uses the input sRGB image for restoring the tone when reconstructing an sRGB image back from a RAW image. Here, for the smooth tone restoration of CycleISP, we apply the same blur kernel used to create the blurry RAW image to the input sharp sRGB image, rather than using the input sharp sRGB image directly. InvISP uses a single normalizing flow-based invertible network, resulting in near-perfect reconstruction quality for cyclic reconstruction. However, its quality significantly degrades when the intermediate RAW images are altered.

(a) D90 → D7000 (b) D40 → A7R3

Figure S2. Qualitative results of camera-to-camera transfer.

While our method outperforms all the other synthetic dataset generation processes both in PSNR and SSIM, it still achieves lower performance than the upper bound model trained using the RealBlur-J training set. We emphasize that the performance gap between the upper bound and ours is partly due to the existence of remaining photometric misalignment in the blurry and sharp image pairs in the RealBlur-J dataset. The sharp and blurry images of the RealBlur-J dataset were captured by different cameras, so they have slightly different tones. While the postprocessing process of the RealBlur-J dataset applies photometric alignment to mitigate this issue, the images in the dataset still have remaining tone difference, which could only be learned from the RealBlur-J training set. Dataset synthesis methods that synthesize blurry images using only sharp images are unable to depict such tone difference between different cameras and, in fact, there is no need to depict such tone differences for the purpose of deblurring. Fig. S1 shows a qualitative comparison. The deblurring model trained with ParamISP visually outperforms each deblurring model trained with other methods, including the upper bound RealBlur-J.

S2.2. Camera-to-Camera Transfer

Given an sRGB image, ParamISP can manipulate the image as if it was taken by a different camera using the inverse and forward ISP networks trained on the different camera. Fig. S2 qualitatively shows the camera-to-camera transfer results of ParamISP. The resulting camera-transferred images (2nd and 4th images) show color tone changes from the input images (1st and 3rd images) without any noticeable artifacts.

S3. Input Features for LocalNet and GlobalNet

It is reported that leveraging the gradient map and color histogram maps improves the ISP network performance by several previous works [6–8]. In our preliminary experiments, we also find a similar finding. Based on this, we design our LocalNet and GlobalNet to be fed additional input features as well as an input image. As additional input features, we include a gradient map, a soft histogram map, and an over-exposure mask to improve the ISP network perfor-

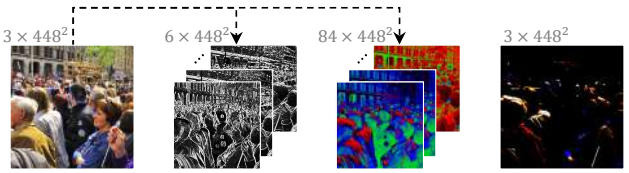

Figure S3. Input features of LocalNet and GlobalNet.

Input Features	w/o A	w/o B	w/o C	Full
PSNR↑	34.32	34.40	34.29	**34.77**
SSIM↑	0.9693	0.9665	0.9677	**0.9712**

Table S2. Ablation study on the impact of each input feature. A, B, and C represent gradient map, soft histogram, and over-exposure mask, respectively.

mance (Fig. S3). For the gradient map, we apply the Sobel filter [5] on an input image and compute per-channel gradient maps in vertical and horizontal directions, resulting in a 6-channel gradient map. For the soft histogram map, we compute the soft histogram [8], for which we measure the relative distance between each channel value of a pixel and the center of histogram bins. In practice, we use 28 histogram bins, resulting in an 84-channel soft histogram map. We also include an over-exposure mask as a hint for restoring pixels of range-clipped values, where we compute the mask by setting its values as $10\max(x-\tau, 0)$ where x is a pixel value of an input image, and τ is a threshold. We use 0.9 as the threshold in our implementation.

Ablation Study To validate the effects of the input features, we conduct an ablation study on RAW reconstruction using the D7000 images of the RAISE dataset [4]. Tab. S2 shows a quantitative ablation study on the input features of LocalNet and GlobalNet. To analyze only the effects of the input features, we use our model without ParamNet as the baseline (4th column). We prepare our baseline with its three model variants, where LocalNet and GlobalNet in each model variant do not use each one of the three input features.

It may be unnecessary to explicitly provide hand-crafted features such as image gradients and soft histograms, as a network can learn to extract such features from an input image. However, without these features, the network may not fully exploit its capacity to learn features more useful for local and global non-linear operations, resulting in low reconstruction quality (1st and 2nd columns). Furthermore, discarding an over-exposure mask may waste the network capacity in estimating and restoring pixels of range-clipped values, resulting in decreased reconstruction performance (3rd column). Additionally, in the first and second rows of Tab. S6, we describe the results of experiments conducted with various cameras and forward ISP networks to assess the impact of input features.

Operation	A	B	$C\times1$	$C\times2$	$C\times3$	$C\times4$	$C\times5$
PSNR↑	32.70	32.77	32.87	32.96	33.27	**33.66**	33.50
SSIM↑	0.962	0.961	0.961	0.962	0.963	0.965	**0.967**

Table S3. Ablation study on the effects of the global adjustment operation of GlobalNet. A and B represent the 3×6 polynomial mapping function of CIE XYZ Net [1] and the 3×10 quadratic transformation of DeepISP [11], respectively, while $C\times N$ denotes N pairs of gamma correction and quadratic transformation (Ours).

Camera model	A7R3[9]	D7000[4]	D90[4]	D40[4]	S7[11]
Training #	7766	4600	1700	26	50
Validation #	200	200	100	-	20
Testing #	1000	1000	400	50	150

Table S4. Statistics of our dataset used for ParamISP.

S4. Global Adjustment Operation of GlobalNet

In this section, we verify the effect of the global adjustment operations of GlobalNet. To this end, we prepare variants of ParamISP with different global adjustment operations, and train them using the D7000 training images of the RAISE dataset [4]. Then, we evaluate their performances using the D7000 test set (Tab. S3). In this evaluation, we include the global adjustment operations of previous methods [1, 11] as well as different numbers of gamma correction and quadratic transformation operations. Tab. S3 shows that our global tone adjustment operation substantially improves the performance in PSNR and SSIM.

S5. Training Strategy

Datasets we use three datasets consisting of RAW and sRGB image pairs captured from multiple cameras: the RAISE dataset [4] from Nikon D7000, D90, and D40, the RealBlur dataset [9] from Sony A7R3; and the S7 ISP dataset [11] from Samsung Galaxy S7. The statistics of each dataset are shown in Tab. S4. We extract camera parameters from the EXIF metadata [12] included in JPEG images.

Pre-training with Images from Diverse Cameras To achieve high-quality reconstruction, we pre-train our models using datasets of multiple cameras as if they were captured by a single camera model. We then fine-tune the models for our target camera. Despite the differences across different camera models, we find that this two-stage training substantially improves the ISP performance as the ISP models can learn common knowledge on the ISP operations.

To validate our two-stage training approach, we present a quantitative ablation study result in Tab. S7. In the table, 'Generic', 'Individual', and 'Generic+individual' mean models trained using multiple camera datasets, models trained using only target camera datasets, and models trained using our two-stage training scheme, respectively. All the 'Generic', 'Individual' and 'Generic+individual'

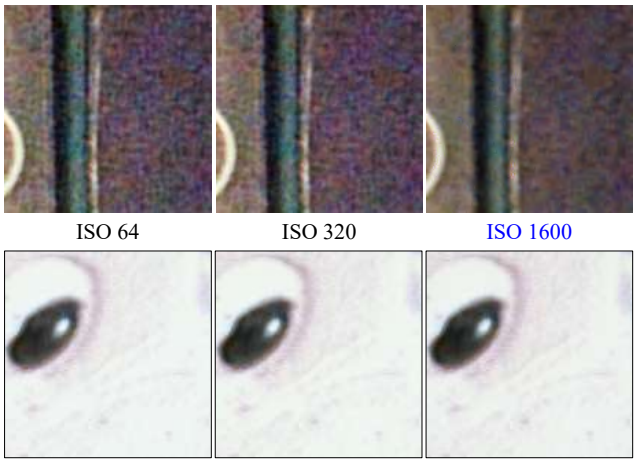

Figure S4. Example of sRGB reconstruction with modified optical parameters (sensitivity and exposure time) using the S7 ISP dataset [11]. The blue text represents the ground-truth value.

models are without ParamNet. We also include our final model 'ParamISP' trained using our two-stage training scheme in the table.

In the table, the 'Individual' models show higher RAW and sRGB reconstruction performance than the 'Generic' models on average as the 'Generic' models cannot properly learn the behaviors of specific camera models. The table also shows that the 'Generic+individual' models achieve higher performance than both 'Generic' and 'individual' models as they can exploit common knowledge on the camera ISP operations across various camera models, and at the same time, they can accurately learn the behaviors of specific camera models. Finally, our full models (ParamISP) outperform all the other models thanks to ParamNet.

Optimal Performance of Each Module While ParamISP features a modularized network architecture where each module has specific objectives, all the modules are jointly trained in an end-to-end fashion utilizing a reconstruction loss. Instead, we may explicitly train each module to serve its intended purpose. Here, we compare these two training approaches.

Given that ParamNet takes only optical parameters as input, and that GlobalNet performs only global adjustment operations, it is clear that ParamNet and GlobalNet are trained to serve their respective purposes. On the other hand, LocalNet may be trained to perform global operations as well as local ones. To explicitly train LocalNet and GlobalNet for their respective purposes, we may 1) train GlobalNet without LocalNet, and 2) fix GlobalNet and train LocalNet. We found that this sequential training results in a RAW reconstruction performance of 33.62dB, which is almost the same as that of the joint training (33.66dB). For clarity, ParamNet was excluded from this experiment. The results suggest that although each module could be explicitly trained for its specific function, our joint training approach suffices to effectively train ParamISP.

Otical Params	A	B	C	D	GT
PSNR↑	34.25	35.53	35.59	35.99	**36.21**
SSIM↑	0.9636	0.9682	0.9703	0.9709	**0.9724**

Table S5. Reconstruction quality of ParamISP with respect to varying optical parameters. A, B, C, and D represent incorrect sensitivity, exposure time, aperture size, and focal length, respectively. GT represents ground-truth. ParamISP achieves the best reconstruction quality for ground-truth optical parameters, while the quality degrades for incorrect parameters, indicating that ParamISP can correctly reflect the adaptive behavior of real-world ISPs.

S6. ParamNet & Optical Parameters

In Sec. 4.1 of the main paper, we analyze the impact of each optical parameter on performance in Tab. 2. To supplement the experimental results in the main paper, we present additional qualitative and quantitative analyses here.

We first verify whether ParamNet operates to reflect the characteristics of optical parameters. As shown in Fig. S4, we manipulate the values of optical parameters and observe changes in visual results. Note that increasing the exposure-related optical parameters of ParamNet, such as aperture size, is not equivalent to increasing the actual exposure. For instance, a manipulated high ISO value for the ISP does not mean that the final processed image should be brightened. Instead, it tells the ISP that its input RAW data is captured with a high ISO value, which results in more noise. The ISP can then adapt its operations, such as increasing the denoising strength. ParamISP operates in the same way as well. As the ISO value increases, the strength of denoising increases (1st row), and as the exposure time increases, saturated areas are restored more effectively (2nd row). This experimental result shows that ParamISP can precisely mimic real-world ISP operations that change according to the optical parameters.

We also present a quantitative analysis. In this analysis, we measure the reconstruction performance of ParamISP against various optical parameters. If ParamISP can accurately replicate the adaptive behavior of a real-world ISP, it is expected to attain optimal reconstruction quality with the ground-truth optical parameters, while the quality should diminish with incorrect parameters. To this end, we use the D7000 test images of the RAISE dataset [4] and their optical parameters. Specifically, for each optical parameter of an image, we randomly change its value and measure its reconstruction quality. Tab. S5 shows a result. In the table, significant performance drops are observed when incorrect values are used for optical parameters. This result indicates that ParamISP can correctly mimic the adaptive behavior of real-world ISPs.

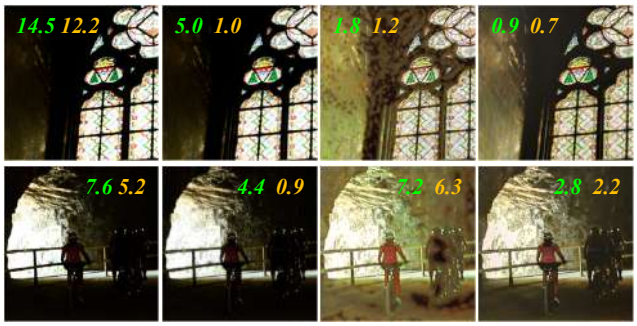

(a) LDR Input (b) CycleISP (c) InvISP (d) ParamISP

Figure S5. HDR reconstruction results of over-exposed regions. Green: proportion of the pixels with values ≥ 250. Yellow: proportion of the pixels with values $= 255$. The results show that our method produces a higher-quality HDR image with more details and also demonstrates a significant reduction in overly bright areas numerically.

S7. Additional Results

We provide additional detailed quantitative results to supplement the experimental results in the main paper: an ablation study on the effects of input features and the proposed ParamNet (Tab. S6), the training strategy (Tab. S7), and comparison on RAW & sRGB reconstruction (Tab. S8). The first two results supplement the experimental results in Sec. 4.1 of the main paper, while the third one supplements Sec. 4.2. Furthermore, we show additional qualitative results on HDR reconstruction (Fig. S5 & Fig. S6), sRGB-to-RAW reconstruction (Fig. S8), and RAW-to-sRGB reconstruction (Fig. S9). In all qualitative results, ParamISP shows visually better results compared to other methods, confirming its superior performance.

We also report a quantitative comparison (sRGB-to-RAW) using the official pretrained models provided by the authors on the Sony A7R3 dataset [9] (Ours: 48.33 (dB), CIE XYZ Net: 27.86, InvISP: 26.43, CycleISP: 25.20). It is worth noting that the official pretrained models of the previous methods were trained on different cameras than the target camera, which explains their lower performance. Fig. S7 shows qualitative results. Our model, trained and evaluated on the Sony A7R3 dataset, demonstrates minimal reconstruction errors. This indicates the importance of training neural ISP models on the target camera, as ISPs are dependent on the specific characteristics of cameras.

S8. Network Architecture

We visualize detailed network architectures for LocalNet (Fig. S10), GlobalNet (Fig. S11), and ParamNet (Fig. S12).

(a) LDR Input (b) CycleISP (c) InvISP (d) ParamISP

Figure S6. Qualitative examples of HDR reconstruction.

GT XYZ Net InvISP CycleISP ParamISP

Figure S7. Qualitative results obtained by performing sRGB-to-RAW reconstruction using official pretrained models. We show error maps between the reconstructed and ground-truth (GT) RAW images. The GT RAW image in this figure is demosaicked for visualization.

References

[1] M. Afifi, A. Abdelhamed, A. Abuolaim, A. Punnappurath, and M. S. Brown. Cie xyz net: Unprocessing images for low-level computer vision tasks. *IEEE Transactions on Pattern Analysis and Machine Intelligence (TPAMI)*, 44(9):4688–4700, 2021. 3, 7

[2] T. Brooks, B. Mildenhall, T. Xue, J. Chen, D. Sharlet, and J. T. Barron. Unprocessing images for learned raw denoising. In *Proceedings of the IEEE Conference on Computer Vision and Pattern Recognition (CVPR)*, 2019. 7

[3] Liangyu Chen, Xiaojie Chu, Xiangyu Zhang, and Jian Sun. Simple baselines for image restoration. In *Proceedings of the European conference on computer vision (ECCV)*, 2022. 1, 2

[4] D.-T. Dang-Nguyen, C. Pasquini, V. Conotter, and G. Boato. Raise: A raw images dataset for digital image forensics. In *Proceedings of the 6th ACM multimedia systems conference (MMSys)*, 2015. 3, 4, 7

[5] N. Kanopoulos, N. Vasanthavada, and Robert L. Baker. Design of an image edge detection filter using the sobel operator. *IEEE Journal of Solid-State Circuits (JSSC)*, 23(2): 358–367, 1988. 3

[6] S. Lin and L. Zhang. Determining the radiometric response function from a single grayscale image. In *Proceedings of the IEEE Conference on Computer Vision and Pattern Recognition (CVPR)*, 2005. 2

[7] S. Lin, J. Gu, S. Yamazaki, and H. Shum. Radiometric calibration from a single image. In *Proceedings of the IEEE Conference on Computer Vision and Pattern Recognition (CVPR)*, 2004.

[8] Y.-L. Liu, W.-S. Lai, Y.-S. Chen, Y.-L. Kao, M.-H. Yang, Y.-Y. Chuang, and J.-B. Huang. Single-image hdr reconstruction by learning to reverse the camera pipeline. In *Proceedings of the IEEE Conference on Computer Vision and Pattern Recognition (CVPR)*, 2020. 2, 3

[9] J. Rim, H. Lee, J. Won, and S. Cho. Real-world blur dataset for learning and benchmarking deblurring algorithms. In *Proceedings of the European Conference on Computer Vision (ECCV)*, 2020. 2, 3, 5, 7

[10] J. Rim, G. Kim, J. Kim, J. Lee, S. Lee, and S. Cho. Realistic blur synthesis for learning image deblurring. In *Proceedings of the European Conference on Computer Vision (ECCV)*, 2022. 2

[11] E. Schwartz, R. Giryes, and A. M. Bronstein. Deepisp: Toward learning an end-to-end image processing pipeline. *IEEE Transactions on Image Processing (TIP)*, 28(2):912–923, 2018. 3, 4, 7

[12] Tsurozoh Tachibanaya. Description of exif file format. `http://www.fifi.org/doc/jhead/exif-e.html`, 2001. 3

[13] Y. Xing, Z. Qian, and Q. Chen. Invertible image signal processing. In *Proceedings of the IEEE Conference on Computer Vision and Pattern Recognition (CVPR)*, 2021. 2, 7

[14] S. W. Zamir, A. Arora, S. Khan, M. Hayat, F. S. Khan, M.-H. Yang, and L. Shao. Cycleisp: Real image restoration via improved data synthesis. In *Proceedings of the IEEE Conference on Computer Vision and Pattern Recognition (CVPR)*, 2020. 2, 7

	Components	D7000 [4]		D90 [4]		D40 [4]		S7 [11]		A7R3 [9]		**Average**	
		PSNR	SSIM	PSNR	SSIM	PSNR	SSIM	PSNR	SSIM	PSNR	SSIM	PSNR	SSIM
sRGB → RAW	Ours (w/o Input Features & ParamNet)	33.66	0.9646	34.50	0.9551	44.87	0.9879	34.51	0.9074	44.66	0.9892	38.44	0.9608
	+Input Features	34.77	0.9712	34.98	0.9672	44.95	0.9847	34.45	0.9063	46.72	0.9912	39.17	0.9641
	+ParamNet w/o dropout	35.64	0.9702	36.26	0.9724	45.41	0.9858	34.81	0.9007	47.47	0.9922	39.92	0.9643
	+w/ dropout	**36.21**	**0.9724**	**36.31**	**0.9731**	**45.73**	**0.9883**	**35.14**	**0.9115**	**47.80**	**0.9922**	**40.24**	**0.9675**
RAW → sRGB	Ours (w/o Input Features & ParamNet)	29.12	0.9399	29.46	0.9544	38.81	0.9843	28.48	0.7593	44.46	0.9806	34.07	0.9237
	+Input Features	29.21	0.9381	29.49	0.9558	39.08	0.9840	28.42	0.7635	44.39	0.9805	34.12	0.9244
	+ParamNet w/o dropout	29.87	0.9421	30.39	0.9639	39.11	0.9836	28.43	0.7668	44.63	0.9808	34.49	0.9274
	+w/ dropout	**29.89**	**0.9422**	**30.50**	**0.9664**	**39.63**	**0.9849**	**28.60**	**0.7690**	**44.78**	**0.9815**	**34.68**	**0.9288**

Table S6. Ablation study on the effects of input features and the proposed ParamNet. Each result was trained and evaluated using a specific camera only.

	Strategy	D7000 [4]		D90 [4]		D40 [4]		S7 [11]		A7R3 [9]		**Average**	
		PSNR	SSIM	PSNR	SSIM	PSNR	SSIM	PSNR	SSIM	PSNR	SSIM	PSNR	SSIM
sRGB → RAW	Generic	34.62	0.9689	35.61	0.9738	41.37	0.9796	34.65	0.9082	44.04	0.9871	38.06	0.9635
	Individual	34.77	0.9712	34.98	0.9672	44.95	0.9847	34.45	0.9063	46.72	0.9912	39.17	0.9641
	Generic+individual	36.47	0.9758	36.59	0.9796	45.75	**0.9879**	34.99	0.9118	47.18	0.9920	40.20	0.9694
	ParamISP (Gen + Ind)	**38.49**	**0.9809**	**37.06**	**0.9810**	**45.97**	0.9877	**35.20**	**0.9125**	**48.33**	**0.9930**	**41.01**	**0.9710**
RAW → sRGB	Generic	28.71	0.9262	28.44	0.9447	34.90	0.9685	28.06	0.7580	39.51	0.9603	31.92	0.9115
	Individual	29.21	0.9381	29.49	0.9558	39.08	0.9840	28.42	0.7635	44.39	0.9805	34.12	0.9244
	Generic+individual	31.51	0.9491	29.50	0.9535	38.97	0.9831	28.42	0.7716	44.95	0.9823	34.67	0.9279
	ParamISP (Gen + Ind)	**34.14**	**0.9628**	**30.83**	**0.9670**	**39.54**	**0.9844**	**29.02**	**0.7868**	**45.51**	**0.9841**	**35.81**	**0.9370**

Table S7. Ablation study on the effects of the training strategy. 'Generic', 'Individual', and 'Generic+individual' mean models trained using multiple camera datasets, models trained using only target camera datasets, and models trained using our two-stage training scheme, respectively. All the 'Generic', 'Individual' and 'Generic+individual' models are without ParamNet. We also include our final model 'ParamISP' trained using our two-stage training scheme in the table.

	Method	D7000 [4]		D90 [4]		D40 [4]		S7 [11]		A7R3 [9]		**Average**	
		PSNR	SSIM	PSNR	SSIM	PSNR	SSIM	PSNR	SSIM	PSNR	SSIM	PSNR	SSIM
sRGB → RAW	UPI [2]	20.67	0.7854	26.57	0.8623	22.05	0.7679	29.98	0.8482	30.48	0.9368	25.95	0.8401
	CIE XYZ Net [1]	30.04	0.9461	32.62	0.9521	38.57	0.9809	33.24	0.8918	36.42	0.9779	34.18	0.9498
	CycleISP [14]	35.52	0.9740	35.85	0.9786	42.83	0.9831	34.55	0.9056	45.35	0.9916	38.82	0.9666
	InvISP [13]	33.48	0.9685	35.39	0.9747	45.08	0.9866	34.29	0.9095	47.14	0.9924	39.08	0.9663
	ParamISP (Ours)	**38.49**	**0.9809**	**37.06**	**0.9810**	**45.97**	**0.9877**	**35.20**	**0.9125**	**48.33**	**0.9930**	**41.01**	**0.9710**
RAW → sRGB	UPI [2]	18.81	0.6326	20.30	0.8010	16.01	0.7649	20.05	0.4205	19.37	0.5324	18.91	0.6303
	CIE XYZ Net [1]	26.76	0.8703	27.61	0.9183	34.84	0.9635	27.63	0.6978	37.19	0.9396	30.81	0.8779
	InvISP [13]	30.20	0.9393	28.89	0.9448	37.86	0.9816	28.96	0.7862	43.93	0.9786	33.97	0.9261
	ParamISP (Ours)	**34.14**	**0.9628**	**30.83**	**0.9670**	**39.54**	**0.9844**	**29.02**	**0.7868**	**45.51**	**0.9841**	**35.81**	**0.9370**

Table S8. Quantitative comparison on RAW & sRGB reconstruction. Note that CycleISP is not included in this comparison because it needs an input sRGB image for sRGB reconstruction.

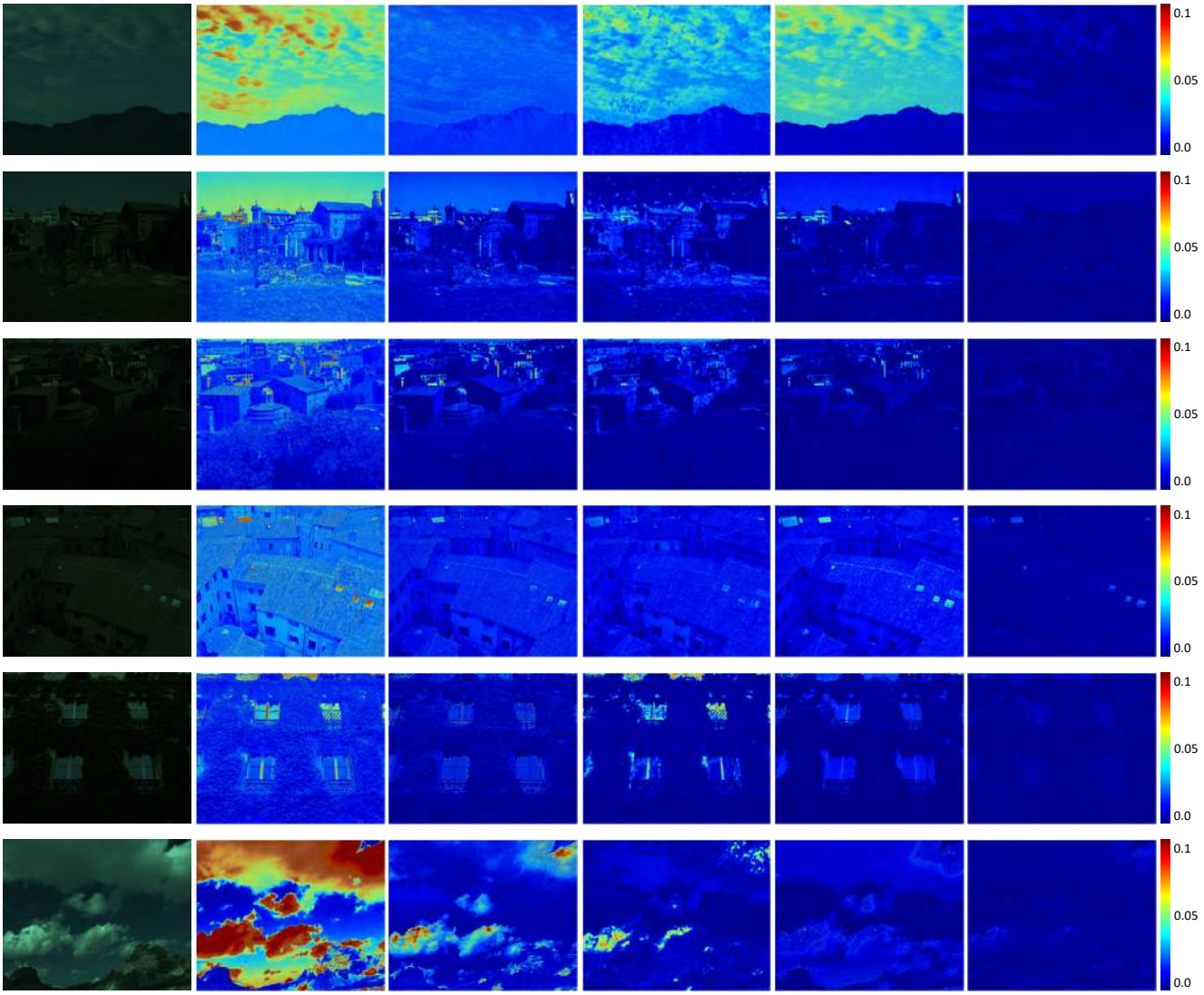

(a) Ground truth (b) UPI (c) CIE XYZ Net (d) InvISP (e) CycleISP (f) ParamISP (Ours)

Figure S8. sRGB-to-RAW reconstruction. We show error maps between reconstructed and GT RAW images.

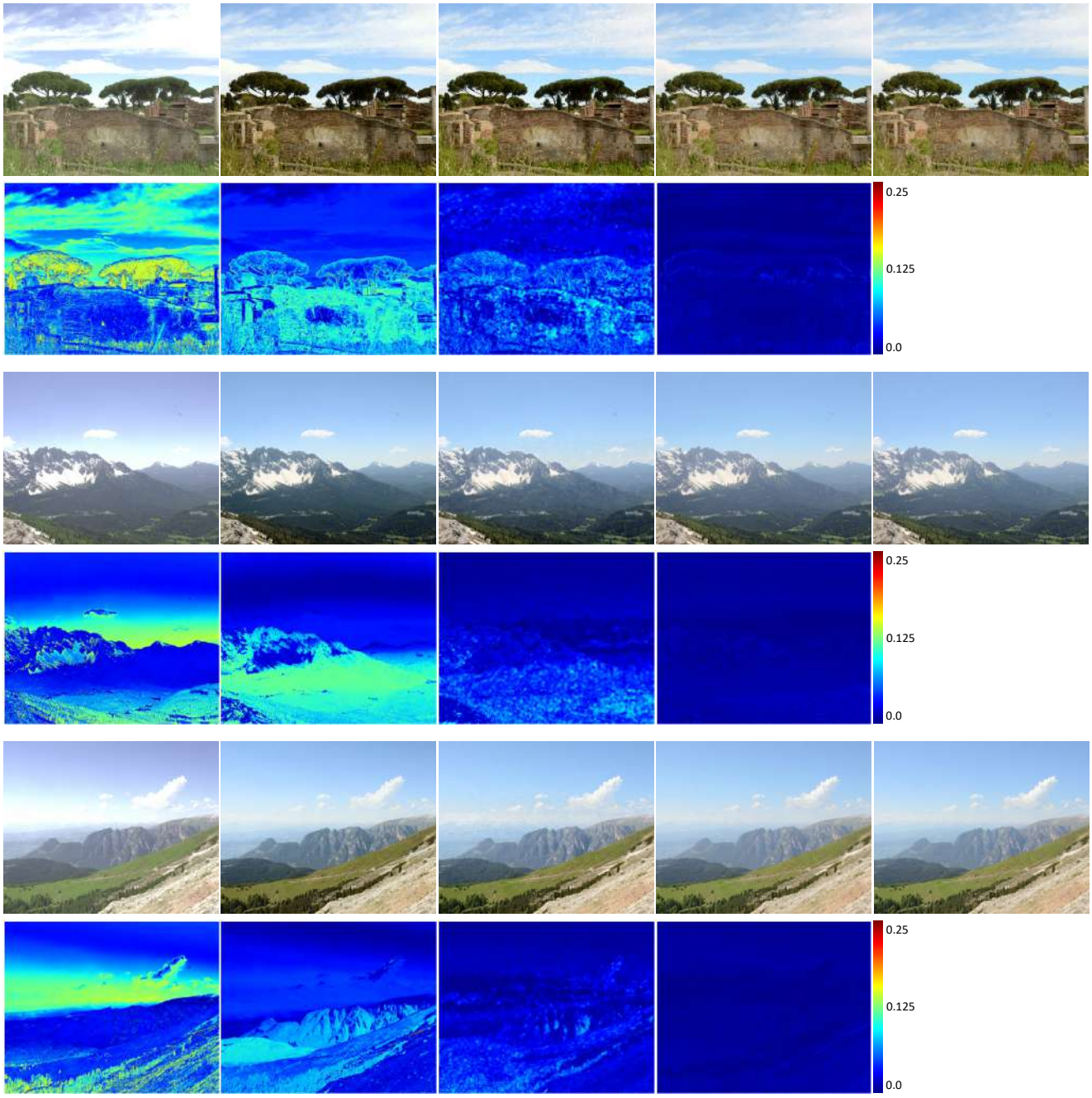

(a) UPI (b) CIE XYZ Net (c) InvISP (d) ParamISP (Ours) (e) Ground truth

Figure S9. RAW-to-sRGB reconstruction. We show error maps between reconstructed and GT sRGB images.

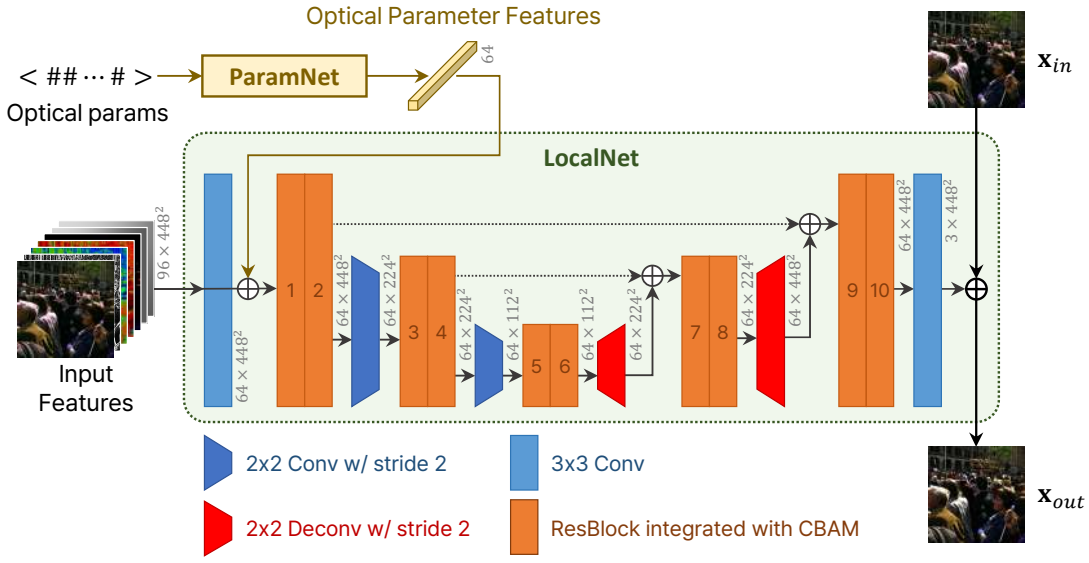

(a) LocalNet

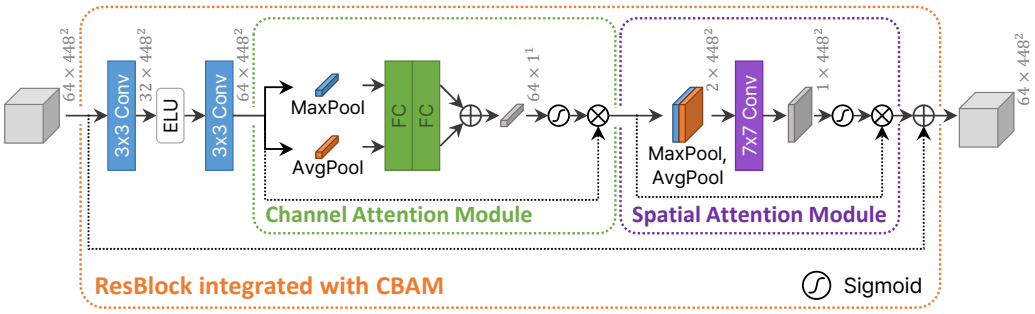

(b) ResBlock integrated with CBAM

Figure S10. Detailed architecture of LocalNet.

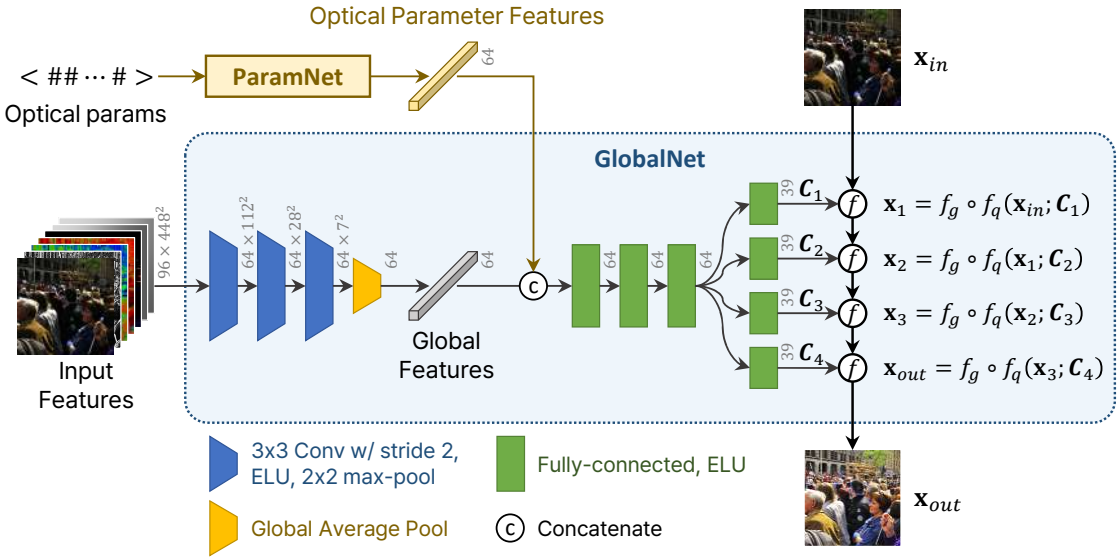

Figure S11. Detailed architecture of GlobalNet.

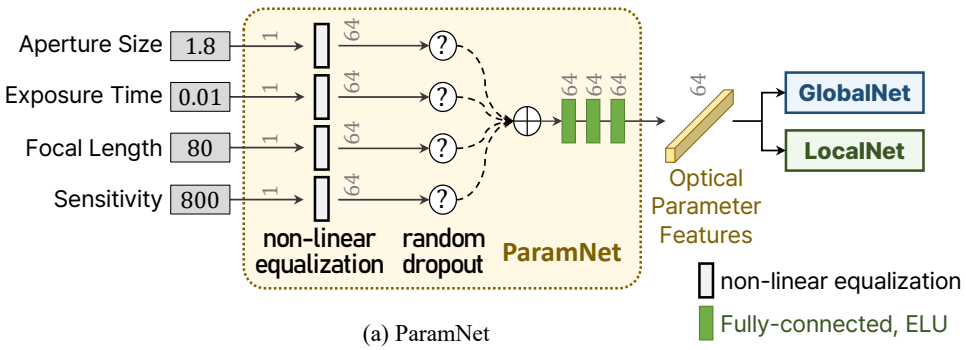

(a) ParamNet

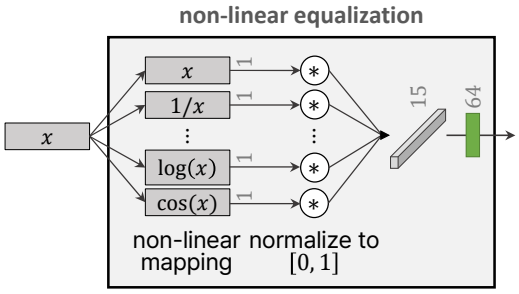

(b) Visualization of non-linear equalization

Figure S12. Detailed architecture of ParamNet.